

## RESEARCH ARTICLE

# SWATH-MS based proteomic profiling of pancreatic ductal adenocarcinoma tumours reveals the interplay between the extracellular matrix and related intracellular pathways

Ekene Emmanuel Nweke<sup>1\*</sup>, Previn Naicker<sup>2</sup>, Shaun Aron<sup>3</sup>, Stoyan Stoychev<sup>2</sup>, John Devar<sup>1</sup>, David L. Tabb<sup>4</sup>, Jones Omshoro-Jones<sup>1</sup>, Martin Smith<sup>1</sup>, Geoffrey Candy<sup>1</sup>

**1** Department of Surgery, Faculty of Health Sciences, University of the Witwatersrand, Johannesburg, South Africa, **2** Department of Biosciences, Council for Scientific and Industrial Research, Pretoria, South Africa, **3** Sydney Brenner Institute for Molecular Bioscience, University of the Witwatersrand, Johannesburg, South Africa, **4** Bioinformatics Unit, South African Tuberculosis Bioinformatics Initiative, Division of Molecular Biology and Human Genetics, Department of Biomedical Sciences, Stellenbosch University, Cape Town, South Africa

\* [ekene.nweke@wits.ac.za](mailto:ekene.nweke@wits.ac.za)



## OPEN ACCESS

**Citation:** Nweke EE, Naicker P, Aron S, Stoychev S, Devar J, Tabb DL, et al. (2020) SWATH-MS based proteomic profiling of pancreatic ductal adenocarcinoma tumours reveals the interplay between the extracellular matrix and related intracellular pathways. *PLoS ONE* 15(10): e0240453. <https://doi.org/10.1371/journal.pone.0240453>

**Editor:** Eithne Costello, University of Liverpool, UNITED KINGDOM

**Received:** June 11, 2020

**Accepted:** September 27, 2020

**Published:** October 13, 2020

**Copyright:** © 2020 Nweke et al. This is an open access article distributed under the terms of the [Creative Commons Attribution License](https://creativecommons.org/licenses/by/4.0/), which permits unrestricted use, distribution, and reproduction in any medium, provided the original author and source are credited.

**Data Availability Statement:** The proteomic data files described in this study have been deposited to the ProteomeXchange Consortium via the PRIDE partner repository (83) with the dataset identifier (PXD019549).

**Funding:** The study was funded by the Council for Scientific and Industrial Research and the South African Medical Research Council through a grant awarded to the Wits Common Epithelial Cancer

## Abstract

Pancreatic cancer accounts for 2.8% of new cancer cases worldwide and is projected to become the second leading cause of cancer-related deaths by 2030. Patients of African ancestry appear to be at an increased risk for pancreatic ductal adenocarcinoma (PDAC), with more severe disease and outcomes. The purpose of this study was to map the proteomic and genomic landscape of a cohort of PDAC patients of African ancestry. Thirty tissues (15 tumours and 15 normal adjacent tissues) were obtained from consenting South African PDAC patients. Optimisation of the sample preparation method allowed for the simultaneous extraction of high-purity protein and DNA for SWATH-MS and OncoArray SNV analyses. We quantified 3402 proteins with 49 upregulated and 35 downregulated proteins at a minimum 2.1 fold change and FDR adjusted p-value (q-value)  $\leq 0.01$  when comparing tumour to normal adjacent tissue. Many of the upregulated proteins in the tumour samples are involved in extracellular matrix formation (ECM) and related intracellular pathways. In addition, proteins such as EMIL1, KBTB2, and ZCCHV involved in the regulation of ECM proteins were observed to be dysregulated in pancreatic tumours. Downregulation of pathways involved in oxygen and carbon dioxide transport were observed. Genotype data showed missense mutations in some upregulated proteins, such as MYPN, ESTY2 and SERPINB8. Approximately 11% of the dysregulated proteins, including ISLR, BP1, PTK7 and OLFL3, were predicted to be secretory proteins. These findings help in further elucidating the biology of PDAC and may aid in identifying future plausible markers for the disease.

Research Centre. DLT was supported in part by a Strategic Health Innovation Partnership (SHIP) grant from the South African (SA) Department of Science and Technology (DST) and the SA Medical Research Council (SAMRC) to Gerhard Walzl. GC is funded by The Cancer Association of South Africa (CANSA). The funders had no role in study design, data collection and analysis, decision to publish, or preparation of the manuscript.

**Competing interests:** The authors have declared that no competing interests exist.

## Introduction

Pancreatic ductal adenocarcinoma (PDAC) accounts for 85% of all pancreatic cancers. World-wide, the incidence and mortality rates of PDAC are rising compared to other cancers [1]. Despite current therapeutic strategies, the survival rate is dismal, with a five-year survival rate of 8% [2]. These poor statistics are chiefly due to late detection, allowing for invasion and metastasis of cancer, and therapeutic resistance. In multiracial countries such as the United States of America, African Americans have increased incidence and poorer survival rates compared to other ethnicities. Although this has been largely attributed to social factors such as smoking, alcohol consumption, obesity and diabetes mellitus, current studies have determined genetics as an underlying factor [3–5].

The normal pancreatic tissue comprises mostly of exocrine (acinar and ductal) cells therefore, PDAC arises from acinar and ductal cells. The tumour microenvironment (TME) of PDAC plays a role in enabling chemotherapeutic resistance, cancer cell proliferation, invasion, migration and metastasis. It is characterised by a dense extracellular matrix (ECM) structure, stromal cells, cancer-associated fibroblasts and immune cells [6–10]. The overexpression of ECM proteins exacerbates PDAC tumourigenesis, fostering tumour growth. Pancreatic cancer cells secreting ECM proteins such as collagen and fibronectin, were found to have increased proliferation and were desensitized to chemotherapeutic drugs such as gemcitabine [11–14]. Hence, there is a need for the identification of novel proteins involved in the ECM formation that could be potential chemotherapeutic targets and biomarkers of PDAC.

Mass spectrometry-based technologies have proven useful in the identification of proteins with important roles in PDAC progression [15]. Sequential window acquisition of all theoretical fragment ion spectra (SWATH) is a label-free application of mass spectrometry (MS), suitable for discovery proteomics where hundreds or thousands of proteins are quantified at high analyte throughput and reproducibility [16, 17].

In the present study, protein and DNA were simultaneously extracted from the same tissue samples, which allowed SWATH-MS and OncoArray single nucleotide variation (SNV) profiling of tissues obtained from resectable (stage I and II) South African PDAC patients who underwent a Whipple procedure. Several significantly differentiated proteins were identified, many of which were enriched in the extracellular matrix formation and related intracellular pathways.

## Methods

### Ethics statement

The Human Research Ethics Committee of the University of Witwatersrand approved this study (HREC- M150778). Each patient gave written informed consent for sample collection and recording of demographic and clinical data.

### Patient recruitment and sample collection

Biopsy samples were obtained from 15 consenting South African patients (aged between 53–95 years old) with histologically confirmed PDAC undergoing the Whipple procedure and admitted to the hepatopancreatobiliary unit at the Chris Hani Baragwanath Academic Hospital (Johannesburg, South Africa) from January 2016 to June 2019. The study further included only patients of African ancestry that were treatment-naïve and excluded those with tumours other than from the pancreas. Patients recruited were considered representative of the population as samples were obtained from approximately equal number of females (46.7%) and males (53.3%). Additionally, the majority (80.2%) of the population in South Africa are of

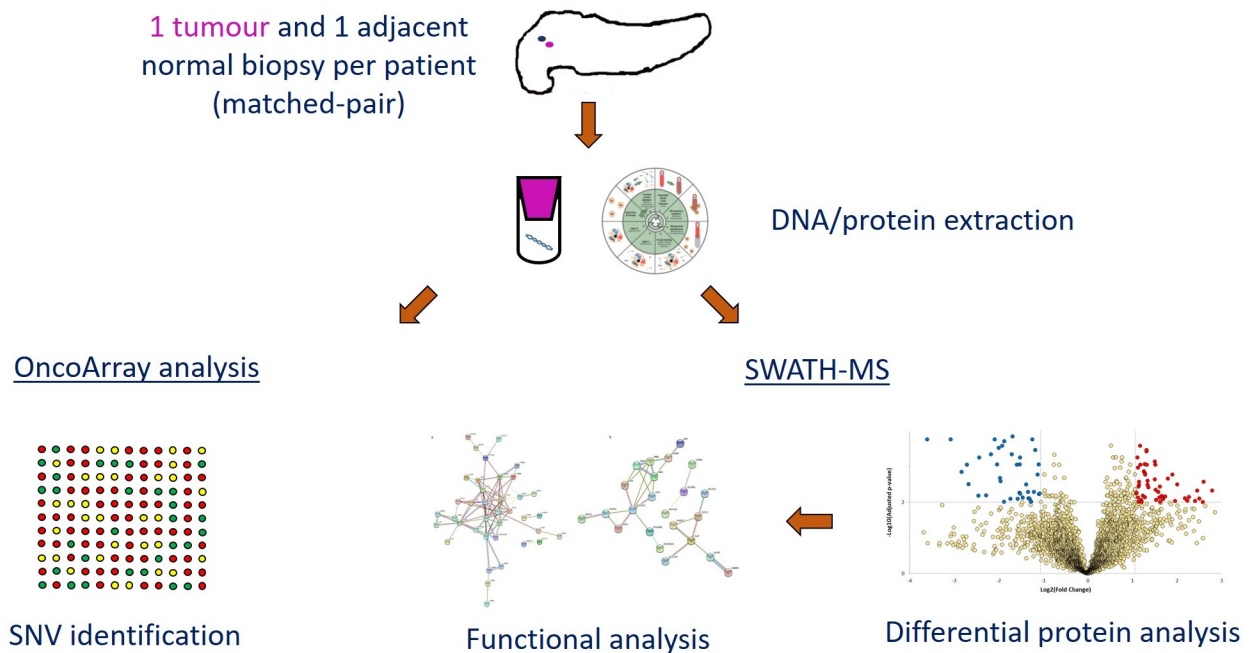


**Fig 1. Overview of study workflow, from sample collection to functional analysis.** Fifteen tumour biopsies and corresponding adjacent were obtained from consenting patients. SWATH-MS and Oncoarray analysis were performed using extracted protein and DNA, respectively. Functional analysis was further conducted on dysregulated proteins.

<https://doi.org/10.1371/journal.pone.0240453.g001>

African ancestry. One core tumour biopsy obtained from the head of the pancreas and one adjacent ‘normal’ tissue (> 2cm away from the tumour) were obtained (30 samples) and immediately frozen at  $-80^{\circ}\text{C}$  (S1 Table). The overview of the study workflow is shown in Fig 1.

### Tissue processing

Tissues (15–35mg) were homogenised in 600 $\mu\text{l}$  of ATL lysis buffer (Qiagen Hilden, Germany) supplemented with 40mM—dithiothreitol (VWR Pennsylvania, United States), using a Tissue Ruptor (Qiagen). The homogenised solution was centrifuged at 14 000g for 3 mins to remove any micro-tissue particulate from the solution. From the recovered lysate 180 $\mu\text{l}$  was taken for DNA purification.

### Protein preparation for mass spectrometry

The remainder of the lysate was incubated with four parts pre-chilled acetone for 30 min at  $-20^{\circ}\text{C}$ . The mixture was centrifuged at 14 000g at  $4^{\circ}\text{C}$  for 10 min and the resultant pellet was washed with ice-cold ethanol. The pellet was resuspended in 50mM Tris-HCl pH 8.0 containing 4% sodium dodecyl sulphate (SDS) and a Roche complete™ EDTA-free protease inhibitor cocktail. The protein concentration was measured using the Pierce Bicinchoninic assay (Thermo Fisher Scientific, Massachusetts, USA). Aliquots of protein solution were then stored at  $-80^{\circ}\text{C}$  until further processing.

Protein samples were thawed and 20 $\mu\text{g}$  per sample was reduced with 10mM dithiothreitol at  $37^{\circ}\text{C}$  for 30 min and alkylated with 40mM iodoacetamide at room temperature in the dark for 30 min. The samples were then purified of detergents and salts using MagReSyn™ HILIC microparticles (ReSyn Biosciences Edenvale, South Africa) in a 96 deep-well plate for automated sample preparation of 12 samples in parallel using the KingFisher Duo™ system

(Thermo Fisher Scientific), as previously described [18]. Briefly, magnetic hydrophilic affinity microparticles (200 $\mu$ l, 200 $\mu$ g) were equilibrated in 200 $\mu$ l of 100mM ammonium acetate pH 4.5 containing 15% acetonitrile (MeCN). Microparticles were then transferred to 100 $\mu$ l of protein binding solution (each protein sample adjusted to 50 $\mu$ l using 4% SDS and added to 50 $\mu$ l of 200mM ammonium acetate pH 4.5 containing 30% MeCN) and mixed for 30 min at room temperature. The captured proteins were washed twice in 200 $\mu$ l of 95% MeCN and transferred to 200 $\mu$ l of 25mM ammonium bicarbonate containing 2 $\mu$ g of sequencing grade trypsin (Promega, Madison, USA) and mixed for 4 hrs digestion at 37°C. The automated on-bead protein capture, clean-up and digest protocol was programmed using BindIt software v4.0 (Thermo Fisher Scientific) and is available upon request ([info@resynbio.com](mailto:info@resynbio.com)) and further described in S1 Fig. Resultant peptides were dried and stored at -80°C before Liquid Chromatography-MS analysis.

### Liquid Chromatography-Mass Spectrometry (LC-MS) data acquisition

Approximately 1 $\mu$ g of tryptic peptides per sample was analysed using a Dionex Ultimate 3000 RSLC system coupled to an AB Sciex 6600 TripleTOF mass spectrometer (AB Sciex, Massachusetts, USA). For data-dependent acquisition (DDA, used for spectral library building), tumour and normal samples were each pooled in their respective groups and spiked with Biognosys iRT retention time peptide standards. Four injection replicates of each group were acquired ( $n = 8$ ). For SWATH, each sample was injected once. Peptide samples were inline de-salted using an Acclaim PepMap C18 trap column (75 $\mu$ m  $\times$  2cm; 2 min at 5 $\mu$ l.min<sup>-1</sup> using 2% Acetonitrile, ACN/0.2% FA). Trapped peptides were gradient eluted and separated on an Acclaim PepMap C18 RSLC column (75 $\mu$ m  $\times$  15cm, 2 $\mu$ m particle size) at a flow-rate of 0.5 $\mu$ l.min<sup>-1</sup> with a gradient of 4–40% B over 60 min (A: 0.1% FA; B: 80% ACN/0.1% FA). For DDA, precursor (MS) scans were acquired from  $m/z$  400–1500 (2<sup>+</sup>–5<sup>+</sup> charge states) using an accumulation time of 250ms followed by 80 fragment ion (MS/MS) scans, acquired from  $m/z$  100–1800 with 25ms accumulation time each. For SWATH, precursor scans ranged from  $m/z$  400 to 900 using 100 variable-width windows that overlapped by 0.5 Da, and fragment ions were acquired from  $m/z$  100–1800 with 25ms accumulation time per window.

### Liquid Chromatography-Mass Spectrometry (LC-MS) data analysis

Raw DDA files (.wiff),  $n = 8$ , were included in a combined search using Protein Pilot software v5.0.2.0 (AB Sciex, Massachusetts, USA), against a database of human reference proteome contained in SwissProt (Accessed 9 June 2019) supplemented with sequences of common contaminants and iRT peptide retention time standards (Biognosys Schlieren, Switzerland). This searched data file was imported into Skyline software v19.1 [19] with peptide features extracted to build a spectral library. A cut-off score of 0.994 (from Protein Pilot report) corresponding to 1% local peptide false discovery rate (FDR) was applied for a library building, with fixed carbamidomethylation of cysteine and variable N-terminal acetylation being the only allowable modifications. The minimum peptide length was 7 and the maximum 36 amino acids and enzyme for digestion set as trypsin with one allowable missed cleavage. The built spectral library contained 141 775 transitions matching to 19 861 peptides and 3413 proteins. Decoy entries were generated by shuffling the peptide sequence, with 141 775 decoy transitions and 19 861 decoy peptides added.

SWATH data files (.wiff),  $n = 30$ , were centroided and converted to mzML format using the msconvert tool in the ProteoWizard software suite v3.0.19217 [20]. The converted data files were imported into Skyline and matched to the spectral library for correct assignment of the mass spectra. A fragment ion mass tolerance of 0.5m/z was employed for library matching,

with a minimum of three and maximum of six of the most intense product ions being selected. The b and y ions with +1 and +2 charge states matching to peptides with +2, +3 and +4 charge states were allowed and product ions from b3 to the last ion were allowed for selection. The iRT peptides were used to align retention times across the dataset using the score to run regression. A 2 min window around the predicted retention time was used to assist in identification. A peak scoring model was trained using mProphet [21] and the decoy peptides generated from the spectral library. All peaks were re-integrated using this model. The MSstats [22] group comparison plugin was implemented within Skyline to perform quantitative analysis. Relative protein abundance across the normal adjacent and tumour experimental groups was measured using the MSstats group comparison which employs a linear mixed effects regression model. Statistical significance is inferred using adjusted p-values (q-values) based on multiple hypothesis correction using the Benjamini-Hochberg method [23]. A normalisation method (equalise medians) was applied for the comparisons across the experimental groups. The MSstats design sample size plugin was used to determine the statistically significant fold change that could be observed based on the desired power, sample number and variability of the dataset. The filtered list of dysregulated proteins was manually inspected within Skyline to verify the quality of the precursors and transitions used for quantitation. Principal component analysis (PCA) was performed using the peptide-level quantification of each sample within Perseus v1.6.5.0 [24].

### DNA extraction and single nucleotide variant array

DNA purification was performed as per the manufacturer's instruction using the Qiagen DNeasy Blood and Tissue kit (Qiagen Hilden, Germany). The total DNA was quantified using a NanoDrop ND-1000 UV spectrophotometer. A ratio of absorbance at 260nm:280nm of >1.9 and 260nm:230nm of >1.5 was observed in all samples. The Illumina Infinium<sup>®</sup> OncoArray-500k Beadchip (Illumina California, United States) was used for single nucleotide variation (SNV) analysis using 200ng of DNA for each sample. The SNV array was conducted as per manufacturer's instruction. GenomeStudio (<https://emea.illumina.com/techniques/microarrays/>) was used to perform clustering and QC of the raw intensity data and the genotype calls were exported as a GenomeStudio report. For downstream analysis, the GenomeStudio report was converted into PLINK [25] format using the *topbottom* module of the H3ABioNet workflow (<https://github.com/h3abionet/h3agwas>). The original dataset consisted of 499 170 SNVs genotyped for 48 samples. Some samples were genotyped in replicate and the replicates were utilised to improve the genotype calling when converting the data to PLINK format.

### Single nucleotide variation (SNV) analysis

The genotype data were subset to include only tumour-normal pairs and replicates were removed, as related samples cannot be used in the association tests. Quality control was conducted on the dataset to remove low-quality SNVs and samples. SNVs with greater than 1% missingness, lower than 1% minor allele frequency and deviations from Hardy-Weinberg Equilibrium were removed. Tumour samples were coded as cases and normal samples coded as controls.

### Functional analysis

REACTOME v70 [26] was applied to show pathway-enrichment analysis of identified dysregulated proteins. A cut-off value of 0.05 and an adjusted p-value based on Benjamini-Hochberg correction test [23] was applied. Cytoscape v3.8.0 [27] with the STRING [28] plug-in was used

to show network interaction between dysregulated proteins. For the STRING analyses, a high-confidence protein interaction score of 0.7 was used and p-values were corrected for multiple testing using Benjamini-Hochberg procedure. ShinyGO v0.61 [29] was used for graphical representation of enriched biological processes/pathways and the Ensembl Variant Effect Predictor tool [30] modelled the consequences of observed SNVs.

## Results

### Differential protein analysis in tumours

Using SWATH-MS, we matched 3413 proteins and 19 861 peptides to our in-house generated spectral library. Peptide quantification was performed on MS2 ion measurements using Skyline [19]. A principal component analysis (PCA) determined the maximum covariance among the samples based on the abundance of all peptides measured in the analysis. This allowed for unsupervised grouping of samples without any manual assignment of groups. The PCA plot (S2 Fig) shows two defined groups of samples in agreement with the two clinically defined groups in the study. The normal adjacent group dataset shows wider distribution compared to the tumour group dataset.

An MSstats group comparison (linear mixed effects model) was performed to determine the relative abundance (fold change) of each quantifiable protein across the tumour and normal adjacent experimental groups. A minimum fold change  $\geq 2.1$  and maximum FDR adjusted p-value (q-value)  $\leq 0.01$  was used to filter proteins that were significantly different between tumour and corresponding normal tissues. The fold change threshold was calculated using the MSstats design sample size plugin within Skyline, based on 0.8 power, 0.01 FDR and 15 replicates per group (S3 Fig). We found 49 upregulated and 35 downregulated proteins in tumours compared to normal adjacent tissues (Fig 2, S2 Table). Across the complete dataset of quantified proteins (3402), 318 are predicted to be secreted based on information from the Human Protein Atlas [31] and Uniprot [32], both accessed on March 24<sup>th</sup> 2020. Among the dysregulated proteins, 78% of the observed differentially expressed proteins (DEPs) have been shown to have prognostic potential in various cancers like colorectal, renal, liver, lung, urothelial, thyroid and endometrial. Furthermore, based on data reported in the Human Protein Atlas database, AP2A2, PLST, PLSI, BLVRB and SLC2A1 were associated with poor 5-year overall survival in pancreatic cancer (S2 Table).

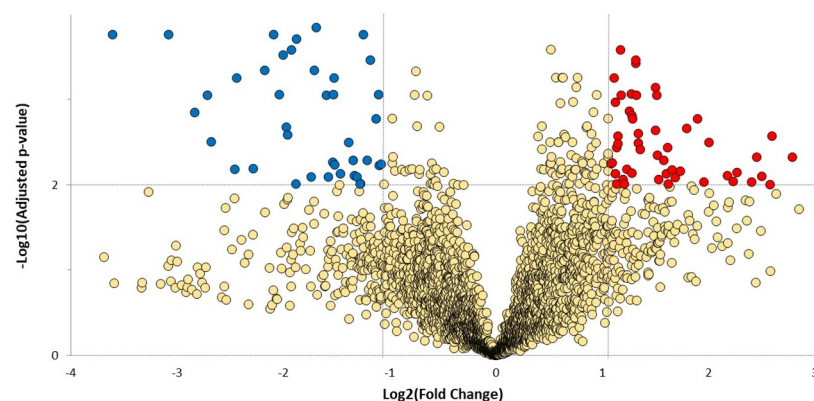


**Fig 2. Volcano plot showing dysregulated proteins.** Blue and red nodes indicate downregulated and upregulated proteins group (based on a minimum fold change  $\geq 2.1$  and a maximum adjusted p-value (q-value)  $\leq 0.01$ ) in tumour compared to normal adjacent, respectively.

<https://doi.org/10.1371/journal.pone.0240453.g002>



**Table 1. Top 10 significantly upregulated pathways in tumour samples.**

Pathway name	False discovery rate	Submitted proteins	Number of submitted proteins found	Total number of proteins in pathway
Recycling pathway of L1	$2.57 \times 10^{-5}$	AP2A2, TBB6, TBB2A, TBB8, ACTG, DPYL2	6	49
Cell-extracellular matrix interactions	$2.02 \times 10^{-4}$	ACTG, ACTN1, LIMS1, ILK	4	18
RHO GTPases activate IQGAPs	$9.95 \times 10^{-4}$	TBB6, TBB2A, TBB8, ACTG	4	32
Translocation of SLC2A4 (GLUT4) to the plasma membrane	$9.95 \times 10^{-4}$	TBB6, TBB2A, TBB8, MYH9, ACTG1	5	72
MHC class II antigen presentation	$1.86 \times 10^{-3}$	AP2A2, TBB6, TBB2A, CATB, CATC	6	142
Cell junction organisation	$2.30 \times 10^{-3}$	PLEC, ACTG, ACTN1, LIMS1, ILK	5	92
Hemostasis	$5.73 \times 10^{-3}$	WDR1, TBB6, TBB2A, SPB8, TBB8, GBB2, GBB1, CAP1, ACTN1, ISLR, AT2B4	11	723
Cell-Cell communication	$5.73 \times 10^{-3}$	PLEC, ACTG, ACTN1, LIMS1, ILK	5	120
Aggrephagy	$1.21 \times 10^{-2}$	TBB6, TBB2A, TBB8	3	44
Platelet activation, signalling and aggregation	$1.21 \times 10^{-2}$	WDR1, ACTN1, ISLR, GBB2, GBB1, CAP1	6	262

Generated from Reactome.

<https://doi.org/10.1371/journal.pone.0240453.t001>

**Table 2. Significantly downregulated pathways in tumour samples.**

Pathway name	False discovery rate	Submitted proteins	Number of submitted proteins found	Total number of proteins in pathway
Erythrocytes take up oxygen and release carbon dioxide	$3.33 \times 10^{-2}$	CAH1, HBB, HBA, B3AT, CAH2	5	16
Metabolism of porphyrins	$3.33 \times 10^{-2}$	HEM2, BLVRB, HEM3	3	73
Factors involved in megakaryocyte development and platelet production	$3.33 \times 10^{-2}$	CAH1, CAH2	2	16

Generated from Reactome.

<https://doi.org/10.1371/journal.pone.0240453.t002>

## Single nucleotide variants observed in tumours

The quality-controlled dataset contained 369,259 SNVs for the 15 paired samples. Although the study was underpowered for detecting statistically significant associations due to the small sample size, we performed a simple linear regression association test on the complete dataset (all tumour versus normal adjacent) to identify SNVs with a difference in allele frequency between the tumour and normal adjacent groups. Top associated results are listed with p-values, although none of these was significant after correcting for multiple testing (S3 Table).

To assess the possible role of SNVs in the regulation of protein levels, the association analysis was re-run on a subset of SNVs extracted based on the gene regions for the previously identified DEPs. The association results were assessed to identify SNVs with a difference in allele frequency between cases (tumour) and controls (normal adjacent). Extraction of SNVs in the gene regions identified from the proteomics results (significantly up and down-regulated proteins) resulted in 912 SNVs. A linear regression association test with this subset of SNVs was conducted and, although no significant difference in allele frequency was observed between the tumour and normal adjacent groups, SNVs were found within some DEPs (S3 Table). We further annotated the types of SNVs (S4 Fig). Sixty-nine percent of the coding SNVs found in DEPs were synonymous variants, while 31% were missense variants. Missense variants were found in *MYPN*, *SERPINB8* (SPB8) and *ESYT2*, which were among the top ten most upregulated proteins in the tumour group.

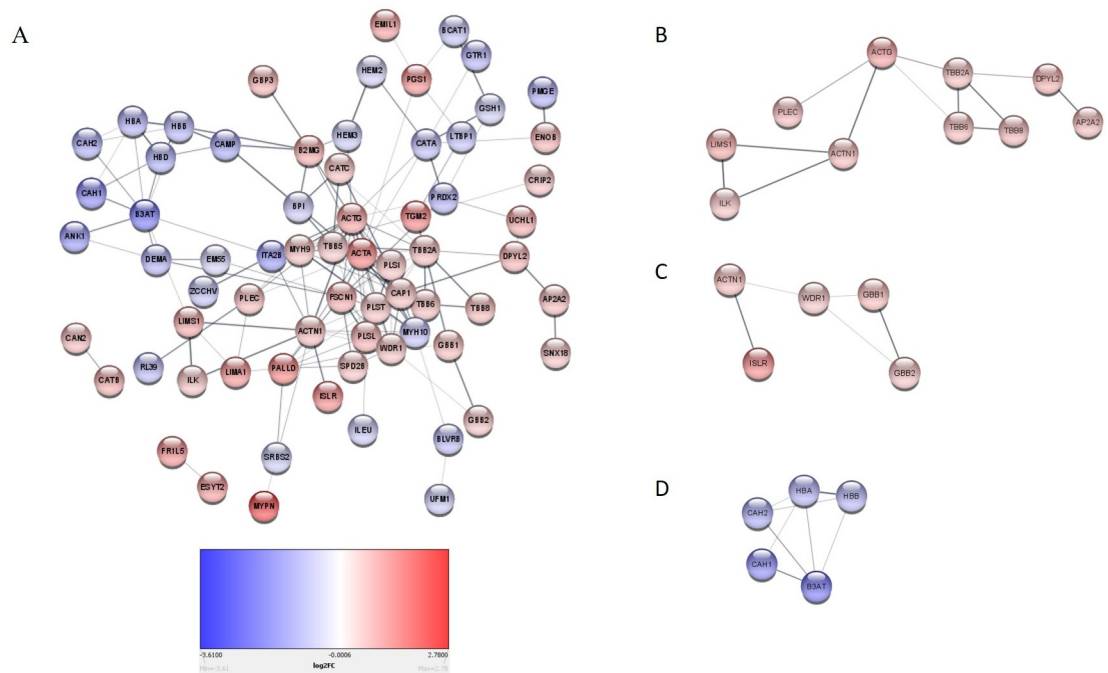


**Fig 4. A Network analysis of dysregulated proteins.** (A) The complete interaction network of the different dysregulated proteins. Proteins involved in Extracellular matrix formation/organisation (B) Recycling pathway of L1, cell-extracellular matrix interactions, cell junction organisation, cell-cell communication, (C) Platelet activation, and (D) O<sub>2</sub>/CO<sub>2</sub> transport are also shown. Red are up-regulated and blue down-regulated proteins as well as that only high confidence interactions were considered when building the String network (fold change cut-off of 0.7).

<https://doi.org/10.1371/journal.pone.0240453.g004>

## Discussion

In this study, we performed proteomic and genomic profiling and identified proteins dysregulated in resected pancreatic tumours obtained from patients of African ancestry. For the first time, to our knowledge, dysregulation of proteins such as EMIL1, KBTB2, and ZCCHV, that are responsible for the regulation of ECM components, were observed in pancreatic tumours. Pathway analysis further showed that the majority of the DEPs were enriched in pathways responsible for/related to extracellular matrix formation.

### Dysregulated proteins implicated in extracellular matrix formation

In this study, we observed that pathways involved in ECM formation and interactions were dysregulated corroborating the findings of several studies [33–36]. The ECM modulates intracellular signalling pathways; consequently, aberrant ECM homeostasis and ECM remodelling can induce and enhance tumorigenesis. Furthermore, there is evidence that the altered expression of ECM components can affect intracellular signalling [37, 38].

The enrichment of ECM-related pathways (Recycling pathway of L1, cell-extracellular matrix interactions, cell junction organisation, cell-cell communication) was due to the upregulation of specific proteins, such as PLEC, ACTN1, LIMS1, and ILK (Table 1, Fig 4(B)). We recently showed that these proteins were also overexpressed at the mRNA level [39] with increased activity of the MAPK and P13K/AKT signalling pathways [39]. Both the MAPK and P13K/AKT signalling pathways are regulated by FAK/SRC activation which results from the interaction of integrin with ECM molecules [40]. Drawing from our studies and literature, Fig 5 shows a schematic of how these pathways interplay in the ECM.

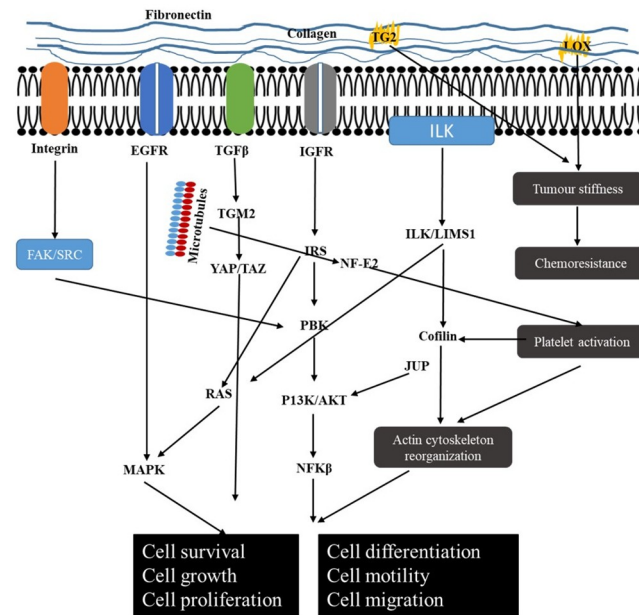


**Fig 5. The schematic interplay between the extracellular matrix and intracellular signalling pathways.** In the tumour microenvironment, pathways associated with the extracellular matrix and intracellular signalling interact with one another. Such pathways include those involved in the signalling of EGFR, IGF, MAPK, integrin, VEGF, TGF $\beta$  and P13/Akt. The cross-talk and activation of these pathways lead to cell survival, growth, proliferation and migration that may enhance tumorigenesis. EGFR (epidermal growth factor receptor); VEGF (vascular endothelial growth factor); TGF $\beta$  (transforming growth factor beta).

<https://doi.org/10.1371/journal.pone.0240453.g005>

The identified dysregulated proteins play important roles in tumorigenesis. PLEC (Plectin) was further found to be up-regulated in squamous cell carcinoma, aiding in the induction of malignant transformation from sinonasal inverted papilloma [41] and has been utilised in pancreatic cancer detection using targeted nanoparticles [42–44]. High expression of ACTN1 (Actinin Alpha 1) promotes cellular migration, invasion and metastasis, by weakening E-cadherin adhesion that ensures cellular integrity [45]. Additionally, ACTN1 has been identified as a key regulator of PDAC progression, using a multidimensional systems-level analysis approach [46]. Increased LIMS1 (LIM and senescent cell antigen-like-containing domain protein 1), a focal adhesion protein, has been associated with poor prognosis in laryngeal and pancreatic cancers [47, 48]. Also, during the knockdown of LIMS1, apoptosis was induced in breast cancer cells [49]. In PDAC, it was found to promote cell survival under hypoxic conditions by activating the AKT/mTOR signalling pathway [47]. ILK (Integrin-linked kinase) which interacts with LIMS1 [50] was also overexpressed in PDAC tumours. One study using neuroblastoma cell lines found that silencing the LIMS1/ILK pathway reduced cellular proliferation, highlighting its potential as a therapeutic target [51].

We also observed the dysregulation of several other proteins, such as TGM2, EMIL1, KBTB2, and ZCCHV, related to the ECM but not enriched in the top significantly dysregulated pathways. Compared to normal adjacent tissues, tumours showed a 6.04-fold increase in Transglutaminase (TGM2) expression, an enzyme involved in extracellular matrix stiffness, by cross-linking collagen 1 fibres [52, 53]. In PDAC tissues, transforming growth factor-beta induces TGM2 expression resulting in the activation of the YAP/TAZ signalling pathway, promoting cellular proliferation, invasion and metastasis [53, 54]. This pathway can be further regulated by ECM stiffness [55–57], characteristic of the extracellular matrix of pancreatic tumours [58, 59]. Another alternative mechanism of tumour stiffness, is mediated by lysyl

oxidase which has been implicated in promoting cancer progression and metastasis [60–64]. EMIL1 is an extracellular matrix glycoprotein that has been identified in both primary and metastatic colon tumours [65]. KBTB2 (Kelch repeat and BTB domain-containing protein 2) is part of the kelch-repeat superfamily that functions in mediating the ubiquitination and degradation of target proteins. Importantly, members of this family are known to mediate cellular adhesion [66, 67]. One member of the family, keap1, was shown to target ectoplasmic specializations indicating interactions with ECM components [68]. ZCCHV (or ZAP) functions in inhibiting viral replication by preventing viral mRNA accumulation [69, 70]. The anti-viral function of ZAP is regulated by Matrin 3, a member of the matrix metalloproteins known to be involved in the degradation of ECM components during tissue and embryo development [71, 72]. This study also found missense mutations in several upregulated proteins, including ESTY2. ESTY2 plays a role in cytoskeleton organisation, which may impact ECM and potentially the overall biology of PDAC cells. In lung cancer cells [73], the short and long variants of ESYT2 were implicated in the cortical distribution of actin and endocytosis, respectively.

Furthermore, we observed that upregulation of platelet activation, signalling and aggregation in tumours (Table 1, Fig 4(C)). Platelet activation results in the release of pro-angiogenic factors (such as VEGF and FGF) and pro-inflammatory markers (such as IL-8 and members of the C-X-C motif ligand family), inducing angiogenesis and inflammation, respectively [74–76]. Of interest, pro-inflammatory factors contribute to the strengthening of the extracellular matrix in the tumour microenvironment [77]. One study showed that elevated mean platelet volume (MPV) correlated with poor survival in pancreatic cancer patients [78]. A major characteristic of platelet activation is the reorganisation of the actin cytoskeleton by cofilin-1 induction [79]. Importantly, WDR1, which was overexpressed in this study, enhances the function of cofilin-1 [80, 81].

In the present study, the downregulation of pathways involved in oxygen and carbon dioxide transport (Table 2, Fig 4(D)) was observed. These pathways were enriched by proteins such as carbonic anhydrase 1 (CAH1) and carbonic anhydrase 2 (CAH2). Carbonic anhydrases are metalloenzymes that play crucial roles in physiological processes including maintaining pH balance, and have been implicated in carcinogenesis [82, 83]. Interestingly, we further observed the downregulation of the glucose transporter, GTR1 (Glut1) (S2 Table), contrary to the findings of other studies that showed its upregulation in pancreatic tumours [84–86]. Although GTR1 was downregulated, ENO3, a key glycolytic enzyme that reversibly converts 2-phosphoglycerate to phosphoenolpyruvate, was overexpressed as observed in another study [87]. Increased glucose metabolism is characteristic of pancreatic cancer cells [88] and can be further regulated and exacerbated in hypoxic conditions [89, 90]. Hypoxia has been linked to tumour stroma stiffness that is characteristic of the extracellular matrix of pancreatic tumours. Additionally, hypoxia is associated with poor survival in pancreatic cancer patients, promoting invasion and metastasis, even in the early stages of the disease, and enabling therapeutic resistance [91].

### Upregulation of proteins involved in cell division and metastasis

Several  $\beta$ -tubulin subtypes including TBB2A, TBB6 and TBB8 were significantly overexpressed in tumour samples (Table 1).  $\beta$ -tubulin combine with  $\alpha$ -tubulin to form microtubules, which play crucial roles in mitotic cell division [92] and cell adhesion [93]. Drugs binding  $\beta$ -tubulin, such as colchicine and paclitaxel, are known to kill cancer cells [94]. Increased expression and mutations in  $\beta$ -tubulin subtypes exacerbate drug resistance in cancer [95–98]. Additionally,  $\beta$ -tubulin is expressed in platelets, aiding in their formation via the NF-E2 pathway [99].

## Conclusion

We have identified significantly dysregulated proteins in resected pancreatic ductal adenocarcinoma tumours obtained from patients of African ancestry using SWATH-MS. Many of these proteins are involved in cell proliferation and in the extracellular matrix formation/organisation, which plays a role in tumour progression and chemo-resistance. These findings warrant the expansion of the discovery dataset described here wherein we will investigate the DEPs in a larger sample cohort. In particular, the detection of secretory proteins in the bloodstream of PDAC patients may be beneficial in the prognosis of the disease. Furthermore, this study utilized bulk tumours which provides knowledge about protein expression patterns and mutations associated with tumours, however it does not account for the individual cell types within the tumour. Thus, future studies should include micro-dissected biopsies allowing for precise analyses of the different cell populations such as stromal, fibroblast and immune cells providing information about contributions of the different cell types.

## Supporting information

**S1 Fig. On-bead based protein capture, clean-up and digestion.** Top: proteins are captured on magnetic hydrophilic affinity microparticles, followed by a high-organic wash to remove contaminants and on-bead digestion by addition of sequencing grade trypsin. Bottom: Plate set-up for automated sample processing in a Thermo Fisher Scientific KingFisher™ Duo Magnetic handling station.

(TIF)

**S2 Fig. Principal component analysis (PCA) showing tumour samples as blue squares and normal adjacent samples as green diamonds.** The PCA plot was generated using peptide abundance data of all peptides analysed per sample.

(TIF)

**S3 Fig. Sample size plot showing the relationship between the number of biological replicates and protein level fold change that can be distinguished based on the current dataset.** A 2.1 fold change can be distinguished in the current study (biological replicates = 15) with statistical power set to 0.8 and false discovery rate (FDR) set to 0.01.

(TIF)

**S4 Fig. Types of variants observed from the list of single nucleotide variants found in (A) All Tumour vs Normal adjacent and (B) Tumour vs Normal adjacent in differentially expressed proteins only.**

(TIF)

**S1 Table. Demographic characteristics of patients recruited for the study.**

(DOCX)

**S2 Table. Differentially expressed proteins (fold change  $\geq 2.1$ ) measured in group comparison.** Positive fold change describes proteins upregulated in the tumour group and negative fold change describes proteins downregulated in tumour compared to the normal adjacent group.

(DOCX)

**S3 Table. Top single nucleotide polymorphisms (SNVs) and associated genes.**

(DOCX)

## Acknowledgments

The authors would like to thank Mr Pavan Baichan for assistance with sample handling.

## Author Contributions

**Conceptualization:** Previn Naicker, Stoyan Stoychev, Martin Smith, Geoffrey Candy.

**Data curation:** Ekene Emmanuel Nweke, Previn Naicker, Shaun Aron, Stoyan Stoychev, John Devar, David L. Tabb, Jones Omoshoro-Jones.

**Formal analysis:** Ekene Emmanuel Nweke, Previn Naicker, Shaun Aron, Stoyan Stoychev, David L. Tabb.

**Funding acquisition:** Previn Naicker, Stoyan Stoychev, Geoffrey Candy.

**Investigation:** Ekene Emmanuel Nweke, Previn Naicker, Stoyan Stoychev, Jones Omoshoro-Jones, Martin Smith, Geoffrey Candy.

**Methodology:** Ekene Emmanuel Nweke, Previn Naicker, Stoyan Stoychev, John Devar, David L. Tabb, Jones Omoshoro-Jones, Martin Smith, Geoffrey Candy.

**Project administration:** Ekene Emmanuel Nweke, Geoffrey Candy.

**Resources:** John Devar, Martin Smith.

**Software:** Previn Naicker.

**Supervision:** Stoyan Stoychev, John Devar, Jones Omoshoro-Jones, Geoffrey Candy.

**Visualization:** Ekene Emmanuel Nweke, Previn Naicker, Shaun Aron.

**Writing – original draft:** Ekene Emmanuel Nweke, Previn Naicker, Shaun Aron, Stoyan Stoychev, David L. Tabb, Geoffrey Candy.

**Writing – review & editing:** Ekene Emmanuel Nweke, Previn Naicker, Shaun Aron, Stoyan Stoychev, John Devar, David L. Tabb, Jones Omoshoro-Jones, Martin Smith, Geoffrey Candy.

## References

1. Bray F, Ferlay J, Soerjomataram I, Siegel RL, Torre LA, Jemal A. Global cancer statistics 2018: GLOBOCAN estimates of incidence and mortality worldwide for 36 cancers in 185 countries. *CA: A Cancer Journal for Clinicians*. 2018; 68: 394–424. <https://doi.org/10.3322/caac.21492>
2. Siegel RL, Miller KD, Jemal A. Cancer statistics, 2018. *CA Cancer J Clin*. 2018; 68: 7–30. <https://doi.org/10.3322/caac.21442> PMID: 29313949
3. Khawja SN, Mohammed S, Silberfein EJ, Musher BL, Fisher WE, Van Buren GI. Pancreatic Cancer Disparities in African Americans. *Pancreas*. 2015; 44: 522–527. <https://doi.org/10.1097/MPA.0000000000000323> PMID: 25872128
4. Silverman DT, Hoover RN, Brown LM, Swanson GM, Schiffman M, Greenberg RS, et al. Why do Black Americans have a higher risk of pancreatic cancer than White Americans? *Epidemiology*. 2003; 14: 45–54. <https://doi.org/10.1097/00001648-200301000-00013> PMID: 12500045
5. Vick AD, Hery DN, Markowiak SF, Brunnicardi FC. Closing the Disparity in Pancreatic Cancer Outcomes: A Closer Look at Nonmodifiable Factors and Their Potential Use in Treatment. *Pancreas*. 2019; 48: 242–249. <https://doi.org/10.1097/MPA.0000000000001238> PMID: 30629027
6. Chu GC, Kimmelman AC, Hezel AF, DePinho RA. Stromal biology of pancreatic cancer. *J Cell Biochem*. 2007; 101: 887–907. <https://doi.org/10.1002/jcb.21209> PMID: 17266048
7. Hwang HJ, Oh M-S, Lee DW, Kuh H-J. Multiplex quantitative analysis of stroma-mediated cancer cell invasion, matrix remodeling, and drug response in a 3D co-culture model of pancreatic tumor spheroids and stellate cells. *J Exp Clin Cancer Res*. 2019; 38: 258. <https://doi.org/10.1186/s13046-019-1225-9> PMID: 31200779

8. Murakami T, Hiroshima Y, Matsuyama R, Homma Y, Hoffman RM, Endo I. Role of the tumor microenvironment in pancreatic cancer. *Ann Gastroenterol Surg.* 2019; 3: 130–137. <https://doi.org/10.1002/ags3.12225> PMID: 30923782
9. Sommariva M, Gagliano N. E-Cadherin in Pancreatic Ductal Adenocarcinoma: A Multifaceted Actor during EMT. *Cells.* 2020; 9. <https://doi.org/10.3390/cells9041040> PMID: 32331358
10. Uzunparmak B, Sahin IH. Pancreatic cancer microenvironment: a current dilemma. *Clin Transl Med.* 2019; 8. <https://doi.org/10.1186/s40169-019-0221-1> PMID: 30645701
11. Amrutkar M, Aasrum M, Verbeke CS, Gladhaug IP. Secretion of fibronectin by human pancreatic stellate cells promotes chemoresistance to gemcitabine in pancreatic cancer cells. *BMC Cancer.* 2019; 19: 596. <https://doi.org/10.1186/s12885-019-5803-1> PMID: 31208372
12. Grzesiak JJ, Bouvet M. The alpha2beta1 integrin mediates the malignant phenotype on type I collagen in pancreatic cancer cell lines. *Br J Cancer.* 2006; 94: 1311–1319. <https://doi.org/10.1038/sj.bjc.6603088> PMID: 16622460
13. Miyamoto H, Murakami T, Tsuchida K, Sugino H, Miyake H, Tashiro S. Tumor-stroma interaction of human pancreatic cancer: acquired resistance to anticancer drugs and proliferation regulation is dependent on extracellular matrix proteins. *Pancreas.* 2004; 28. <https://doi.org/10.1097/00006676-200401000-00006> PMID: 14707728
14. Procacci P, Moscheni C, Sartori P, Sommariva M, Gagliano N. Tumor–Stroma Cross-Talk in Human Pancreatic Ductal Adenocarcinoma: A Focus on the Effect of the Extracellular Matrix on Tumor Cell Phenotype and Invasive Potential. *Cells.* 2018; 7. <https://doi.org/10.3390/cells7100158> PMID: 30301152
15. Kim K, Ahn S, Lim J, Yoo BC, Hwang J-H, Jang W. Detection of Pancreatic Cancer Biomarkers Using Mass Spectrometry. *Cancer Inform.* 2015; 13: 45–53. <https://doi.org/10.4137/CIN.S16341> PMID: 25673969
16. Ludwig C, Gillet L, Rosenberger G, Amon S, Collins BC, Aebersold R. Data-independent acquisition-based SWATH-MS for quantitative proteomics: a tutorial. *Mol Syst Biol.* 2018; 14: e8126. <https://doi.org/10.15252/msb.20178126> PMID: 30104418
17. Gillet LC, Navarro P, Tate S, Röst H, Selevsek N, Reiter L, et al. Targeted data extraction of the MS/MS spectra generated by data-independent acquisition: a new concept for consistent and accurate proteome analysis. *Mol Cell Proteomics.* 2012; 11: O111.016717. <https://doi.org/10.1074/mcp.O111.016717> PMID: 22261725
18. Buthelezi SG, Dirr HW, Chakauya E, Chikwamba R, Martens L, Tsekoa TL, et al. The study of degradation mechanisms of glyco-engineered plant produced anti-rabies monoclonal antibodies E559 and 62-71-3. *PLoS ONE.* 2018; 13: e0209373. <https://doi.org/10.1371/journal.pone.0209373> PMID: 30571707
19. MacLean B, Tomazela DM, Shulman N, Chambers M, Finney GL, Frewen B, et al. Skyline: an open source document editor for creating and analyzing targeted proteomics experiments. *Bioinformatics.* 2010; 26: 966–968. <https://doi.org/10.1093/bioinformatics/btq054> PMID: 20147306
20. Chambers MC, Maclean B, Burke R, Amodei D, Ruderman DL, Neumann S, et al. A cross-platform toolkit for mass spectrometry and proteomics. *Nat Biotechnol.* 2012; 30: 918–920. <https://doi.org/10.1038/nbt.2377> PMID: 23051804
21. Reiter L, Rinner O, Picotti P, Hüttenhain R, Beck M, Brusniak M-Y, et al. mProphet: automated data processing and statistical validation for large-scale SRM experiments. *Nature Methods.* 2011; 8: 430–435. <https://doi.org/10.1038/nmeth.1584> PMID: 21423193
22. Choi M, Chang C-Y, Clough T, Brody D, Killeen T, MacLean B, et al. MSstats: an R package for statistical analysis of quantitative mass spectrometry-based proteomic experiments. *Bioinformatics.* 2014; 30: 2524–2526. <https://doi.org/10.1093/bioinformatics/btu305> PMID: 24794931
23. Benjamini Y, Hochberg Y. Controlling the False Discovery Rate: A Practical and Powerful Approach to Multiple Testing. *Journal of the Royal Statistical Society: Series B (Methodological).* 1995; 57: 289–300. <https://doi.org/10.1111/j.2517-6161.1995.tb02031.x>
24. Tyanova S, Temu T, Sinitcyn P, Carlson A, Hein MY, Geiger T, et al. The Perseus computational platform for comprehensive analysis of (prote)omics data. *Nat Methods.* 2016; 13: 731–740. <https://doi.org/10.1038/nmeth.3901> PMID: 27348712
25. Purcell S, Neale B, Todd-Brown K, Thomas L, Ferreira MAR, Bender D, et al. PLINK: a tool set for whole-genome association and population-based linkage analyses. *Am J Hum Genet.* 2007; 81: 559–575. <https://doi.org/10.1086/519795> PMID: 17701901
26. Fabregat A, Jupe S, Matthews L, Sidiropoulos K, Gillespie M, Garapati P, et al. The Reactome Pathway Knowledgebase. *Nucleic Acids Res.* 2018; 46: D649–D655. <https://doi.org/10.1093/nar/gkx1132> PMID: 29145629

27. S P, M A, O O, B Ns, W Jt, R D, et al. Cytoscape: A Software Environment for Integrated Models of Bio-molecular Interaction Networks. In: Genome research [Internet]. Genome Res; Nov 2003 [cited 20 May 2020]. <https://doi.org/10.1101/gr.1239303> PMID: 14597658
28. Szklarczyk D, Morris JH, Cook H, Kuhn M, Wyder S, Simonovic M, et al. The STRING database in 2017: quality-controlled protein-protein association networks, made broadly accessible. *Nucleic Acids Res.* 2017; 45: D362–D368. <https://doi.org/10.1093/nar/gkw937> PMID: 27924014
29. Ge SX, Jung D, Yao R. ShinyGO: a graphical enrichment tool for animals and plants. *Bioinformatics.* 2019. <https://doi.org/10.1093/bioinformatics/btz931> PMID: 31882993
30. McLaren W, Gil L, Hunt SE, Riat HS, Ritchie GRS, Thormann A, et al. The Ensembl Variant Effect Predictor. *Genome Biol.* 2016; 17: 122. <https://doi.org/10.1186/s13059-016-0974-4> PMID: 27268795
31. Thul PJ, Lindskog C. The human protein atlas: A spatial map of the human proteome. *Protein Sci.* 2018; 27: 233–244. <https://doi.org/10.1002/pro.3307> PMID: 28940711
32. UniProt: a worldwide hub of protein knowledge. *Nucleic Acids Res.* 2019; 47: D506–D515. <https://doi.org/10.1093/nar/gky1049> PMID: 30395287
33. Hosein AN, Brekken RA, Maitra A. Pancreatic cancer stroma: an update on therapeutic targeting strategies. *Nature Reviews Gastroenterology & Hepatology.* 2020; 1–19. <https://doi.org/10.1038/s41575-020-0300-1> PMID: 32393771
34. Tian C, Öhlund D, Rickelt S, Lidström T, Huang Y, Hao L, et al. Cancer Cell-Derived Matrisome Proteins Promote Metastasis in Pancreatic Ductal Adenocarcinoma. *Cancer Res.* 2020; 80: 1461–1474. <https://doi.org/10.1158/0008-5472.CAN-19-2578> PMID: 32029550
35. Tian C, Clauser KR, Öhlund D, Rickelt S, Huang Y, Gupta M, et al. Proteomic analyses of ECM during pancreatic ductal adenocarcinoma progression reveal different contributions by tumor and stromal cells. *Proc Natl Acad Sci U S A.* 2019; 116: 19609–19618. <https://doi.org/10.1073/pnas.1908626116> PMID: 31484774
36. Weniger M, Honselmann KC, Liss AS. The Extracellular Matrix and Pancreatic Cancer: A Complex Relationship. *Cancers (Basel).* 2018; 10. <https://doi.org/10.3390/cancers10090316> PMID: 30200666
37. Hastings JF, Skhinas JN, Fey D, Croucher DR, Cox TR. The extracellular matrix as a key regulator of intracellular signalling networks. *Br J Pharmacol.* 2019; 176: 82–92. <https://doi.org/10.1111/bph.14195> PMID: 29510460
38. Skhinas JN, Cox TR. The interplay between extracellular matrix remodelling and kinase signalling in cancer progression and metastasis. *Cell Adh Migr.* 2018; 12: 529–537. <https://doi.org/10.1080/19336918.2017.1405208> PMID: 29168660
39. Nweke E, Ntwasa M, Brand M, Devar J, Smith M, Candy G. Increased expression of plakoglobin is associated with upregulated MAPK and PI3K/AKT signalling pathways in early resectable pancreatic ductal adenocarcinoma. *Oncology Letters.* 2020 [cited 25 Mar 2020]. <https://doi.org/10.3892/ol.2020.11473> PMID: 32382352
40. Mitra SK, Hanson DA, Schlaepfer DD. Focal adhesion kinase: in command and control of cell motility. *Nat Rev Mol Cell Biol.* 2005; 6: 56–68. <https://doi.org/10.1038/nrm1549> PMID: 15688067
41. Yang Z, Zhang Y, Wang X, Huang J, Guo W, Wei P, et al. Putative biomarkers of malignant transformation of sinonasal inverted papilloma into squamous cell carcinoma. *J Int Med Res.* 2019; 47: 2371–2380. <https://doi.org/10.1177/0300060519838385> PMID: 30991875
42. Chen X, Zhou H, Li X, Duan N, Hu S, Liu Y, et al. Plectin-1 Targeted Dual-modality Nanoparticles for Pancreatic Cancer Imaging. *EBioMedicine.* 2018; 30: 129–137. <https://doi.org/10.1016/j.ebiom.2018.03.008> PMID: 29574092
43. Kelly KA, Bardeesy N, Anbazhagan R, Gurumurthy S, Berger J, Alencar H, et al. Targeted nanoparticles for imaging incipient pancreatic ductal adenocarcinoma. *PLoS Med.* 2008; 5: e85. <https://doi.org/10.1371/journal.pmed.0050085> PMID: 18416599
44. Yang L, Mao H, Cao Z, Wang YA, Peng X, Wang X, et al. Molecular imaging of pancreatic cancer in an animal model using targeted multifunctional nanoparticles. *Gastroenterology.* 2009; 136: 1514–1525. e2. <https://doi.org/10.1053/j.gastro.2009.01.006> PMID: 19208341
45. Kovac B, Mäkelä TP, Vallenius T. Increased  $\alpha$ -actinin-1 destabilizes E-cadherin-based adhesions and associates with poor prognosis in basal-like breast cancer. *PLoS ONE.* 2018; 13: e0196986. <https://doi.org/10.1371/journal.pone.0196986> PMID: 29742177
46. Rajamani D, Bhasin MK. Identification of key regulators of pancreatic cancer progression through multi-dimensional systems-level analysis. *Genome Med.* 2016; 8: 38. <https://doi.org/10.1186/s13073-016-0282-3> PMID: 27137215
47. Huang C, Li Y, Li Z, Xu Y, Li N, Ge Y, et al. LIMS1 Promotes Pancreatic Cancer Cell Survival under Oxygen-Glucose Deprivation Conditions by Enhancing HIF1A Protein Translation. *Clin Cancer Res.* 2019; 25: 4091–4103. <https://doi.org/10.1158/1078-0432.CCR-18-3533> PMID: 30679163

48. Tsinias G, Nikou S, Papadas T, Pitsos P, Papadaki H, Bravou V. High PINCH1 Expression in Human Laryngeal Carcinoma Associates with Poor Prognosis. *Anal Cell Pathol (Amst)*. 2018; 2018: 2989635. <https://doi.org/10.1155/2018/2989635> PMID: 29755929
49. Bhatia A, Muthusamy S, Giridhar K, Goel S. Knockdown of PINCH-1 protein sensitizes the estrogen positive breast cancer cells to chemotherapy induced apoptosis. *Pathol Res Pract*. 2018; 214: 290–295. <https://doi.org/10.1016/j.prp.2017.09.026> PMID: 29079319
50. Tu Y, Li F, Goicoechea S, Wu C. The LIM-only protein PINCH directly interacts with integrin-linked kinase and is recruited to integrin-rich sites in spreading cells. *Mol Cell Biol*. 1999; 19: 2425–2434. <https://doi.org/10.1128/mcb.19.3.2425> PMID: 10022929
51. Saeki N, Saito A, Sugaya Y, Amemiya M, Ono H, Komatsuzaki R, et al. Chromatin Immunoprecipitation and DNA Sequencing Identified a LIMS1/ILK Pathway Regulated by LMO1 in Neuroblastoma. *Cancer Genomics Proteomics*. 2018; 15: 165–174. <https://doi.org/10.21873/cgp.20074> PMID: 29695398
52. Huang L, Xu A-M, Liu W. Transglutaminase 2 in cancer. *American Journal of Cancer Research*. 2015; 5: 2756–2776. PMID: 26609482
53. Lee J, Condello S, Yakubov B, Emerson R, Caprell-Grant A, Hitomi K, et al. Tissue Transglutaminase Mediated Tumor-Stroma Interaction Promotes Pancreatic Cancer Progression. *Clin Cancer Res*. 2015; 21: 4482–4493. <https://doi.org/10.1158/1078-0432.CCR-15-0226> PMID: 26041746
54. Verderio E a. M, Johnson T, Griffin M. Tissue transglutaminase in normal and abnormal wound healing: review article. *Amino Acids*. 2004; 26: 387–404. <https://doi.org/10.1007/s00726-004-0094-4> PMID: 15290345
55. Wang L, Luo J-Y, Li B, Tian XY, Chen L-J, Huang Y, et al. Integrin-YAP/TAZ-JNK cascade mediates atheroprotective effect of unidirectional shear flow. *Nature*. 2016; 540: 579–582. <https://doi.org/10.1038/nature20602> PMID: 27926730
56. Schroeder MC, Halder G. Regulation of the Hippo pathway by cell architecture and mechanical signals. *Semin Cell Dev Biol*. 2012; 23: 803–811. <https://doi.org/10.1016/j.semcdb.2012.06.001> PMID: 22750148
57. Lee HJ, Diaz MF, Price KM, Ozuna JA, Zhang S, Sevick-Muraca EM, et al. Fluid shear stress activates YAP1 to promote cancer cell motility. *Nat Commun*. 2017; 8: 14122. <https://doi.org/10.1038/ncomms14122> PMID: 28098159
58. Nguyen AV, Nyberg KD, Scott MB, Welsh AM, Nguyen AH, Wu N, et al. Stiffness of pancreatic cancer cells is associated with increased invasive potential. *Integr Biol (Camb)*. 2016; 8: 1232–1245. <https://doi.org/10.1039/c6ib00135a> PMID: 27761545
59. Rice AJ, Cortes E, Lachowski D, Cheung BCH, Karim SA, Morton JP, et al. Matrix stiffness induces epithelial–mesenchymal transition and promotes chemoresistance in pancreatic cancer cells. *Oncogenesis*. 2017; 6: e352–e352. <https://doi.org/10.1038/oncsis.2017.54> PMID: 28671675
60. Smith-Mungo LI, Kagan HM. Lysyl oxidase: properties, regulation and multiple functions in biology. *Matrix Biol*. 1998; 16: 387–398. [https://doi.org/10.1016/s0945-053x\(98\)90012-9](https://doi.org/10.1016/s0945-053x(98)90012-9) PMID: 9524359
61. Amendola PG, Reuten R, Erler JT. Interplay Between LOX Enzymes and Integrins in the Tumor Microenvironment. *Cancers (Basel)*. 2019; 11. <https://doi.org/10.3390/cancers11050729> PMID: 31130685
62. Pickup MW, Laklai H, Acerbi I, Owens P, Gorska AE, Chytil A, et al. Stromally derived lysyl oxidase promotes metastasis of transforming growth factor- $\beta$ -deficient mouse mammary carcinomas. *Cancer Res*. 2013; 73: 5336–5346. <https://doi.org/10.1158/0008-5472.CAN-13-0012> PMID: 23856251
63. Baker A-M, Bird D, Lang G, Cox TR, Erler JT. Lysyl oxidase enzymatic function increases stiffness to drive colorectal cancer progression through FAK. *Oncogene*. 2013; 32: 1863–1868. <https://doi.org/10.1038/onc.2012.202> PMID: 22641216
64. Cox TR, Bird D, Baker A-M, Barker HE, Ho MW-Y, Lang G, et al. LOX-mediated collagen crosslinking is responsible for fibrosis-enhanced metastasis. *Cancer Res*. 2013; 73: 1721–1732. <https://doi.org/10.1158/0008-5472.CAN-12-2233> PMID: 23345161
65. Naba A, Clauser KR, Whittaker CA, Carr SA, Tanabe KK, Hynes RO. Extracellular matrix signatures of human primary metastatic colon cancers and their metastases to liver. *BMC Cancer*. 2014; 14: 518. <https://doi.org/10.1186/1471-2407-14-518> PMID: 25037231
66. Heiska L, Carpén O. Src Phosphorylates Ezrin at Tyrosine 477 and Induces a Phosphospecific Association between Ezrin and a Kelch-Repeat Protein Family Member. *J Biol Chem*. 2005; 280: 10244–10252. <https://doi.org/10.1074/jbc.M411353200> PMID: 15623525
67. Velichkova M, Guttman J, Warren C, Eng L, Kline K, Vogl AW, et al. A human homologue of Drosophila kelch associates with myosin-VIIa in specialized adhesion junctions. *Cell Motility*. 2002; 51: 147–164. <https://doi.org/10.1002/cm.10025> PMID: 11921171

68. Spence HJ, Johnston I, Ewart K, Buchanan SJ, Fitzgerald U, Ozanne BW. Krp1, a novel kelch related protein that is involved in pseudopod elongation in transformed cells. *Oncogene*. 2000; 19: 1266–1276. <https://doi.org/10.1038/sj.onc.1203433> PMID: 10713668
69. Wang X, Tu F, Zhu Y, Gao G. Zinc-finger antiviral protein inhibits XMRV infection. *PLoS One*. 2012; 7: e39159. <https://doi.org/10.1371/journal.pone.0039159> PMID: 22720057
70. Zhu Y, Chen G, Lv F, Wang X, Ji X, Xu Y, et al. Zinc-finger antiviral protein inhibits HIV-1 infection by selectively targeting multiply spliced viral mRNAs for degradation. *Proc Natl Acad Sci U S A*. 2011; 108: 15834–15839. <https://doi.org/10.1073/pnas.1101676108> PMID: 21876179
71. Erazo A, Goff SP. Nuclear matrix protein Matrin 3 is a regulator of ZAP-mediated retroviral restriction. *Retrovirology*. 2015; 12: 57. <https://doi.org/10.1186/s12977-015-0182-4> PMID: 26129669
72. Geurts N, Opendakker G, Van den Steen PE. Matrix metalloproteinases as therapeutic targets in protozoan parasitic infections. *Pharmacology & Therapeutics*. 2012; 133: 257–279. <https://doi.org/10.1016/j.pharmthera.2011.11.008> PMID: 22138604
73. de Miguel FJ, Pajares MJ, Martínez-Terroba E, Ajona D, Morales X, Sharma RD, et al. A large-scale analysis of alternative splicing reveals a key role of QKI in lung cancer. *Molecular Oncology*. 2016; 10: 1437. <https://doi.org/10.1016/j.molonc.2016.08.001> PMID: 27555542
74. Gasic GJ, Gasic TB, Stewart CC. Antimetastatic effects associated with platelet reduction. *Proc Natl Acad Sci USA*. 1968; 61: 46–52. <https://doi.org/10.1073/pnas.61.1.46> PMID: 5246932
75. Gay LJ, Felding-Habermann B. Contribution of platelets to tumour metastasis. *Nat Rev Cancer*. 2011; 11: 123–134. <https://doi.org/10.1038/nrc3004> PMID: 21258396
76. Labelle M, Begum S, Hynes RO. Direct signaling between platelets and cancer cells induces an epithelial-mesenchymal-like transition and promotes metastasis. *Cancer Cell*. 2011; 20: 576–590. <https://doi.org/10.1016/j.ccr.2011.09.009> PMID: 22094253
77. Olsson AK, Cedervall J. The pro-inflammatory role of platelets in cancer. *Platelets*. 2018; 29: 569–573. <https://doi.org/10.1080/09537104.2018.1453059> PMID: 29584534
78. Yin J, Wang X, Zhang X, Liu L, Wang R. Mean platelet volume predicts survival in pancreatic cancer patients with synchronous liver metastases. *Sci Rep*. 2018; 8.
79. Dasgupta S, Le A, Haudek S, Entman M, Thiagarajan P. Cofilin-1–Induced Actin Reorganization and Phosphatidylserine Exposure in Platelets. *Blood*. 2014; 124: 4153–4153. <https://doi.org/10.1182/blood.V124.21.4153.4153>
80. Dasgupta SK, Le A, Da Q, Cruz M, Rumbaut RE, Thiagarajan P. Wdr1-Dependent Actin Reorganization in Platelet Activation. *PLoS ONE*. 2016; 11: e0162897. <https://doi.org/10.1371/journal.pone.0162897> PMID: 27627652
81. Rodal AA, Tetreault JW, Lappalainen P, Drubin DG, Amberg DC. Aip1p interacts with cofilin to disassemble actin filaments. *J Cell Biol*. 1999; 145: 1251–1264. <https://doi.org/10.1083/jcb.145.6.1251> PMID: 10366597
82. Nordfors K, Haapasalo J, Korja M, Niemelä A, Laine J, Parkkila A-K, et al. The tumour-associated carbonic anhydrases CA II, CA IX and CA XII in a group of medulloblastomas and supratentorial primitive neuroectodermal tumours: an association of CA IX with poor prognosis. *BMC Cancer*. 2010; 10: 148. <https://doi.org/10.1186/1471-2407-10-148> PMID: 20398423
83. Supuran CT. Carbonic anhydrases: novel therapeutic applications for inhibitors and activators. *Nat Rev Drug Discov*. 2008; 7: 168–181. <https://doi.org/10.1038/nrd2467> PMID: 18167490
84. Sharen G, Peng Y, Cheng H, Liu Y, Shi Y, Zhao J. Prognostic value of GLUT-1 expression in pancreatic cancer: results from 538 patients. *Oncotarget*. 2017; 8: 19760. <https://doi.org/10.18632/oncotarget.15035> PMID: 28178665
85. Lu K, Yang J, Li D-C, He S-B, Zhu D-M, Zhang L-F, et al. Expression and clinical significance of glucose transporter-1 in pancreatic cancer. *Oncol Lett*. 2016; 12: 243–249. <https://doi.org/10.3892/ol.2016.4586> PMID: 27347132
86. Yang H-J, Xu W-J, Guan Y-H, Zhang H-W, Ding W-Q, Rong L, et al. Expression of Glut-1 and HK-II in Pancreatic Cancer and Their Impact on Prognosis and FDG Accumulation. *Translational Oncology*. 2016; 9: 583–591. <https://doi.org/10.1016/j.tranon.2016.08.004> PMID: 27916293
87. Chaika NV, Yu F, Purohit V, Mehla K, Lazenby AJ, DiMaio D, et al. Differential Expression of Metabolic Genes in Tumor and Stromal Components of Primary and Metastatic Loci in Pancreatic Adenocarcinoma. *PLoS ONE*. 2012; 7: e32996. <https://doi.org/10.1371/journal.pone.0032996> PMID: 22412968
88. Yan L, Raj P, Yao W, Ying H. Glucose Metabolism in Pancreatic Cancer. *Cancers (Basel)*. 2019; 11.
89. Liu Z, Jia X, Duan Y, Xiao H, Sundqvist K-G, Permert J, et al. Excess glucose induces hypoxia-inducible factor-1 $\alpha$  in pancreatic cancer cells and stimulates glucose metabolism and cell migration. *Cancer Biol Ther*. 2013; 14: 428–435. <https://doi.org/10.4161/cbt.23786> PMID: 23377827

90. Guillaumond F, Leca J, Olivares O, Lavaut M-N, Vidal N, Berthezène P, et al. Strengthened glycolysis under hypoxia supports tumor symbiosis and hexosamine biosynthesis in pancreatic adenocarcinoma. *PNAS*. 2013; 110: 3919–3924. <https://doi.org/10.1073/pnas.1219555110> PMID: 23407165
91. Erkan M, Kurtoglu M, Kleeff J. The role of hypoxia in pancreatic cancer: a potential therapeutic target? *Expert Rev Gastroenterol Hepatol*. 2016; 10: 301–316. <https://doi.org/10.1586/17474124.2016.1117386> PMID: 26560854
92. Parker AL, Kavallaris M, McCarroll JA. Microtubules and their role in cellular stress in cancer. *Front Oncol*. 2014; 4: 153. <https://doi.org/10.3389/fonc.2014.00153> PMID: 24995158
93. Bershadsky A, Chausovsky A, Becker E, Lyubimova A, Geiger B. Involvement of microtubules in the control of adhesion-dependent signal transduction. *Current Biology*. 1996; 6: 1279–1289. [https://doi.org/10.1016/s0960-9822\(02\)70714-8](https://doi.org/10.1016/s0960-9822(02)70714-8) PMID: 8939572
94. Zhou J, Giannakakou P. Targeting microtubules for cancer chemotherapy. *Curr Med Chem Anticancer Agents*. 2005; 5: 65–71. <https://doi.org/10.2174/1568011053352569> PMID: 15720262
95. Huzil JT, Chen K, Kurgan L, Tuszynski JA. The roles of beta-tubulin mutations and isotype expression in acquired drug resistance. *Cancer Inform*. 2007; 3: 159–181. PMID: 19455242
96. Kelley MJ, Li S, Harpole DH. Genetic Analysis of the  $\beta$ -Tubulin Gene, TUBB, in Non-Small-Cell Lung Cancer. *J Natl Cancer Inst*. 2001; 93: 1886–1888. <https://doi.org/10.1093/jnci/93.24.1886> PMID: 11752014
97. Leandro-García LJ, Leskelä S, Landa I, Montero-Conde C, López-Jiménez E, Letón R, et al. Tumoral and tissue-specific expression of the major human beta-tubulin isotypes. *Cytoskeleton (Hoboken)*. 2010; 67: 214–223. <https://doi.org/10.1002/cm.20436> PMID: 20191564
98. Nami B, Wang Z. Genetics and Expression Profile of the Tubulin Gene Superfamily in Breast Cancer Subtypes and Its Relation to Taxane Resistance. *Cancers (Basel)*. 2018; 10. <https://doi.org/10.3390/cancers10080274> PMID: 30126203
99. Lecine P, Italiano JE, Kim SW, Villeval JL, Shivdasani RA. Hematopoietic-specific beta 1 tubulin participates in a pathway of platelet biogenesis dependent on the transcription factor NF-E2. *Blood*. 2000; 96: 1366–1373. PMID: 10942379